MEMOIRS OF THE SCHOOL OF ENGINEERING, OKAYAMA UNIVERSITY Vol. 6, No. 1, SEPTEMBER 1971

Analysis on Magnetic Characteristics of Three-Phase Core-Type Transformers (Part I: Fundamental Equations and Linear Solutions)

By

Takayoshi NAKATA and Yoshiyuki ISHIHARA

Department of Electrical Engineering

(Received Apr. 30, 1971)

Synopsis

In this paper, we report the procedure to analyse magnetic circuits and give the linear solutions on magnetic characteristics of the three-phase core-type transformer which is composed of the complicated magnetic paths.

First, we explain the construction of cores investigated and normalize the sizes of a core. To analyse these magnetic circuits, we introduced the electrical equivalent circuits and obtained the general fundamental equations for each core. Then, we drew the linear-numerical solutions using an electronic computer, and cleared the relationships between the sizes of a core and the amplitudes and phase angles of fluxes in magnetic paths. Related with the above facts, we investigate the influence of these sizes on the core loss using cores of various quality.

§ 1. Introduction

In a large power transformer-core, ducts are designed perpendicularly to the core-axis in order to necessitate cooling or construction. Therefore, the core is divided into several magnetic paths. In a distribution transformer with wound cores, the core is also divided into several parts due to manufacturing problems. In such cores, the distribution of fluxes differs from that of the usual three-phase core made of a simple magnetic circuit. Consequently, the magnetic characteristics such as core loss, exciting current etc. are going to be modified.

These phenomena have been studied qualitatively by Vidmar etc.[1),2)] for many years. Küchler[3)] has measured the flux waves of individual magnetic paths and the iron loss of the core which is called "*Rahmen construction*", and concluded that the flux densities in the respective paths are about 5% higher than that in the leg and the core loss increases about 10% more than that of a usual core. Yamaguchi[4),5)] has analysed the *Rahmen* core, which consists of three independent magnetic circuits, assuming that the magnetization characteristic is linear.

In consideration of the non-linearity, we have analysed the magnetic characteristics with several kinds of three-phase core which is presently used and consists of complicated magnetic circuits. This paper describes the procedure analysing the magnetic circuits and the linear solutions as the preparatory process to obtain the non-linear solutions. The linear solutions are helpful for understanding a general tendency of the phenomena. This paper also describes the relationships between the core shape and the amplitudes and phase angles of fluxes in magnetic paths. Using these results, the core loss has been calculated and compared with that composed of a simple magnetic circuit.

We emphasize here that the fundamental equations can be used to the case of non-linear solutions. The details of results on non-linear solutions will be reported subsequently.

§ 2. Construction of Transformer Core and Its Sizes

Figure 1 shows the transformer cores which have been investigated and are being used

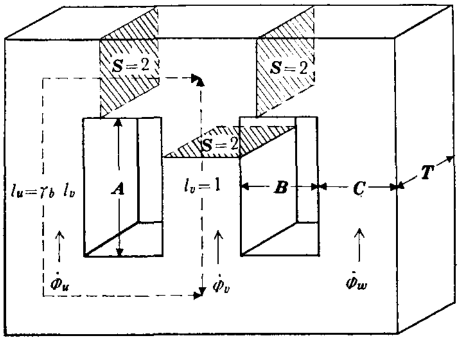

(a) *B-type* core. $\gamma_b = l_u/l_v$

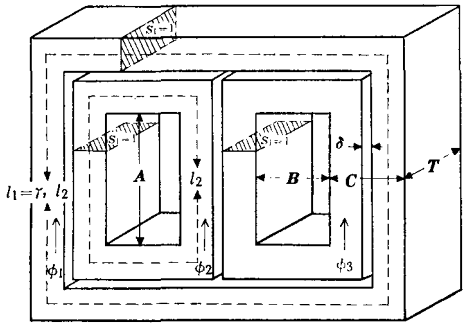

(b) *R3-type* core. $\gamma_r = l_1/l_2$

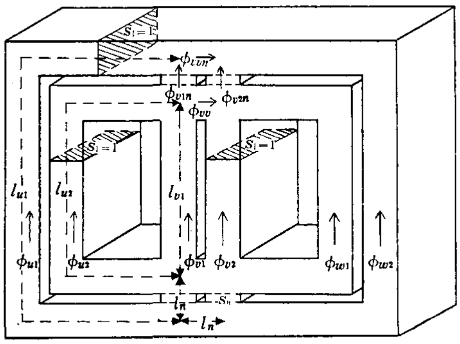

(c) *C10-type* core. $\gamma_s = S_n/S_1$

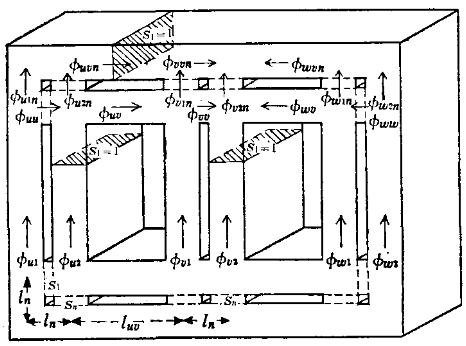

(d) *C20-type* core. $\gamma_s = S_n/S_1$

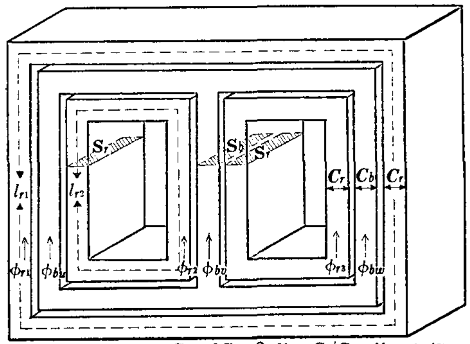

$S_b + 2S_r = 2,\ \gamma_c = C_b/C_r\ ,\ \gamma_s = S_b/S_r$

(e) *R6-type* core.

Fig. 1 Schematic diagrams of transformer-cores.

commonly. Figure 1 (a) shows the most popular construction of three-phase transformer-core which is composed of simple magnetic circuit. The latter is called the "*B-type core*" and is used as a standard which will be compared with the characteristics of other type of cores. The core shown in Fig. 1 (b) is one of so called "*Rahmen constructions*". It is composed of three independent magnetic paths setting a duct in the centre, and is used as a distribution transformer with wound cores as well as a middle power transformer. We designate the core in Fig. 1 (b) as the "*R3*-type*".

The construction illustrated in Fig. 1 (c) of which magnetic characteristics are improved by sacrificing cooling effect at the upper and lower parts of the central leg is named the "*C10-type*". In Fig. 1 (d), the magnetic paths are also coupled at the upper and lower parts of the *U* and *W* legs to each other in order to improve the magnetic characteristics. We call this the "*C20-type*". The core shown in Fig. 1 (e) has two ducts with further cooling effect. It consists of four independent magnetic circuits and is used as a large transformer-core. We call it the "*R6-type*".

In any construction described above, we assume that size and shape of a cut surface of the yoke are equal to those of the leg, and normalize the total sectional area S of the leg

* The core with ducts of which all magnetic paths are coupled magnetically is designated as the *C-type*. The core which consists of independent magnetic circuits is called the *R-type*. A figure X in the "*RX-type*" or "*CX-type*" means the number of branches on equivalent circuit in Fig. 4.

as 2. Excluding the thickness T in the laminated core which has no influence on magnetic characteristics, the factors to determine the core shape are three variables, that is dimensions A and B of the window and width C of the leg. But for convenience of the following calculation, we normalize the mean magnetic path-length l_v of the central leg as 1, and introduce a parameter γ_b. The γ_b is a ratio of mean magnetic path-length l_u of the U leg to that l_v of the V leg (that is, $\gamma_b = l_u/l_v$) as shown in Fig. 1 (a). Further, we introduce a parameter γ_r which is a ratio of mean path-length l_1 of the outer magnetic path to length l_2 of the inner one (that is, $\gamma_r = l_1/l_2$) as shown in Fig. 1 (b). Then, the core shape can be determined by parameters γ_b and γ_r (, $l_v=1$) instead of dimensions A, B and C. The following advantage can be obtained by these normalization; that is, the magnetic characteristics of the *R3-type* core are almost determined only by γ_r. The relation between parameters (γ_b and γ_r) and dimensions (A, B and C) is shown in Fig. 2 and Eqs. (1), (2) and (3). The width δ of core ducts is neglected in these calculations. This assumption may be permissible, because the value of δ is about 6 to 10mm in large transformers commonly used.

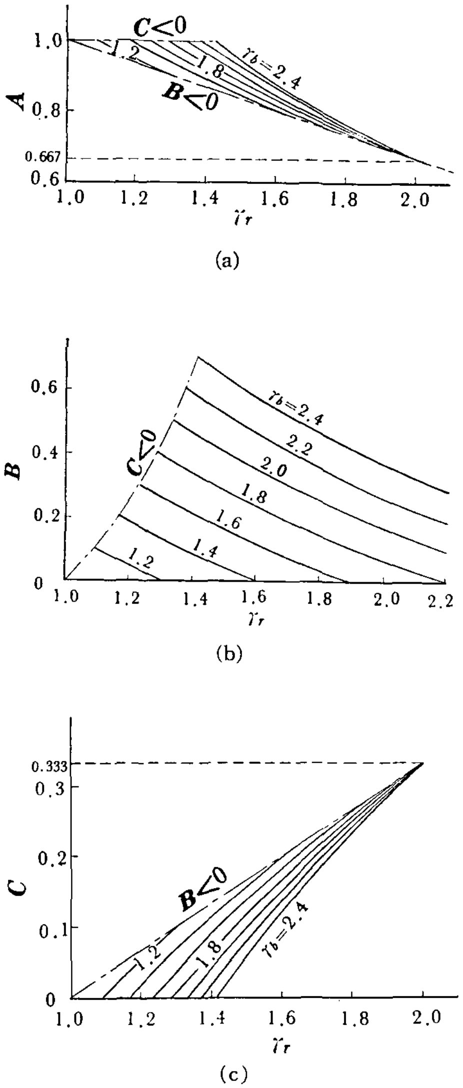

Fig. 2 Relations between core dimensions and parameters.

$$A = \{4 + \gamma_{rb}(2 - \gamma_r)\}/6, \tag{1}$$

$$B = \gamma_{rb}/2 - 1, \tag{2}$$

$$C = \{2 - \gamma_{rb}(2 - \gamma_r)\}/6. \tag{3}$$

Where

$$\gamma_{rb} = (3\gamma_b + 1)/(\gamma_r + 1), \tag{4}$$

$$\gamma_r = l_1/l_2, \tag{5}$$

$$\gamma_b = l_u/l_v. \tag{6}$$

γ_{rb} is equal to l_2, when l_v is normalized as 1. Therefore, it can be understood from Eq. (2) that l_2 is influenced only by the width B of core window.

Figure 2 shows the following tendencies. When the dimension A of the window becomes larger, γ_r becomes smaller, and when C becomes larger, γ_r becomes larger too. When B becomes larger, γ_r becomes smaller while γ_b becomes larger.

In order to examine variations of magnetic characteristics by filling rate at the top and bottom of the V leg, we introduce a parameter γ_s into the *C-type* core. The γ_s is a ratio of effective sectional area S_n of this part to effective sectional area $S_1(=1)$ of the leg-part (that is, $\gamma_s = S_n/S_1$). In the *C20-type* core, the effective sectional area of connecting part at the top and bottom of the U and W legs is S_n too. In the *R6-type* core, we introduce another parameter γ_c which is a ratio of width C_b of the central magnetic path to width C_r of the side path (that is, $\gamma_c = C_b/C_r$). And here, γ_s denotes a ratio of effective sectional area S_b

of the central magnetic path to effective sectional area S_r of the side path (that is, $\gamma_s = S_b/S_r$).

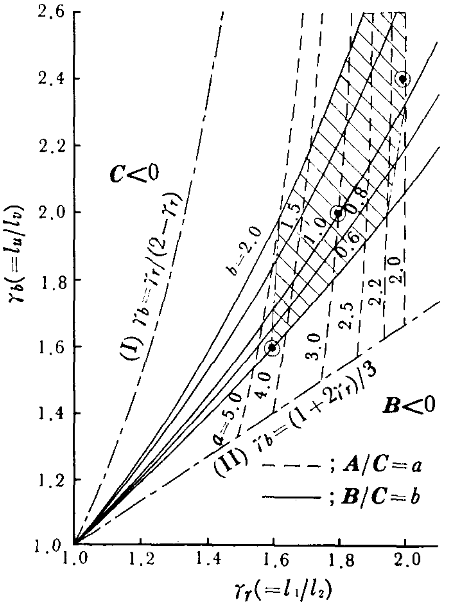

Fig. 3 The usual extent of γ_r and γ_b.

In Fig. 3 the hatched area shows a range ordinarily used in a power transformer. Fig. 3 also shows the relationship between γ_b and γ_r, where A/C and B/C are parameters. In a large transformer, γ_b and γ_r are usually sought in the diagonally upward region of the hatched area due to difficult transportation by a train. In Fig. 3, the curve (I) is the limitting line of $C=0$, and γ_b and γ_r can not exist on the upper side of this curve. The curve (II) is the limitting line of $B=0$, and γ_b and γ_r can not exist on the lower side of this curve. Chain lines in Fig. 2 indicate these limitting conditions.

If γ_b, γ_r and γ_c are given, the mean magnetic length of each branch path in respective type core can be calculated as these functions. In order to calculate the characteristics such as core loss as described later, the combinations of γ_b and γ_r which are shown in Fig. 3 by mark ⊙ are chosen as the typical core shapes.

§ 3. Analysis of Magnetic Circuits

To analyse the magnetic circuits, we make the following assumptions.

(i) The leakage fluxes are negligible.

(ii) There is no flux which passes through the ducts[2),4)].

(iii) The influence of joints between the core sheets can be neglected.

(iv) The flux distribution is uniform in each magnetic path, and the length of magnetic path is expressed by the mean value of all length.

(v) The material is homogeneous throughout of the core.

(vi) The applied voltage of each leg is of the symmetrical three-phase sinusoidal wave.

3.1 Equivalent Circuits

The introduction of electrical equivalent circuits makes us analyse easier magnetic circuits. Figure 4 (a) through (e) are the electrical equivalent circuits corresponded to Fig. 1. The magnetic reluctance R is a function of flux Φ in non-linear circuit, and the following relations exist between them.

$$R\,\Phi = M, \tag{7}$$

$$M = l\, f(B), \tag{8}$$

$$H = f(B). \tag{9}$$

Where M is the magnetomotive force, l is the length of magnetic path, H is the magnetic field intensity, B is the magnetic flux density and $f(B)$ is the functional form of magnetization curve.

For notation of symbols, a capital letter means a maximum value, a small letter means a instantaneous value and the subscripts show the corresponding branch.

For considerations on the equivalent circuit, it is of important facts that in the electric circuit the current flows in proportion to the applied voltage whereas in the magnetic circuit the magnetomotive force arises in proportion to the magnetic flux. Accordingly, in the magnetic circuit a concept simular to a constant-current source applied for the electric circuit is need.

3.2 Fundamental Equations

Applying Kirchhoff's first and second laws to the nodes and loops of the equivalent circuits in Fig. 4 respectively, the Eqs. (10) through (48) are obtained.

(1) R3-Type Core

The following equations are satisfied between leg fluxes and path fluxes.

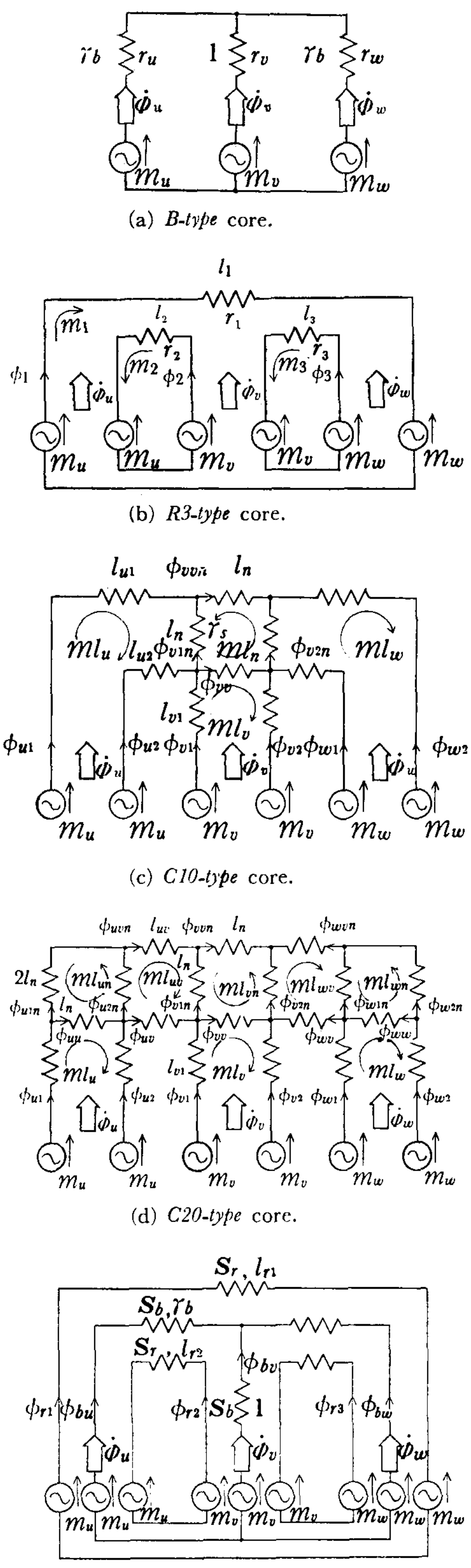

(a) *B-type* core.

(b) *R3-type* core.

(c) *C10-type* core.

(d) *C20-type* core.

(e) *R6-type* core.

Fig. 4 Equivalent circuits for transformer-cores.

$$b_2 = b_1 - \phi_u, \tag{10}$$

$$b_3 = b_1 + \phi_w. \tag{11}$$

By Kirchhoff's second law,

$$\gamma_b f(b_1) + f(b_2) + f(b_3) \equiv 0. \tag{12}$$

(2) C10-Type Core

Corresponding to Eqs. (10) and (11), Eqs. (13) and (14) are obtained.

$$b_{u2} = \phi_u - b_{u1}, \tag{13}$$

$$b_{v2} = \phi_v - b_{v1}. \tag{14}$$

For nodes,

$$b_{vv} = b_{v1} + b_{u2} - \gamma_s\ b_{v1n}, \tag{15}$$

$$b_{vvn} = b_{u1} + \gamma_s\ b_{v1n}, \tag{16}$$

$$b_{w1} = -b_{v2} - b_{vv} + \gamma_s\ b_{v2n}, \tag{17}$$

$$b_{w2} = -b_{vvn} - \gamma_s\ b_{v2n}. \tag{18}$$

For loops,

$$ml_u = l_{u1} f(b_{u1}) - l_{u2} f(b_{u2}) - 2l_n f(b_{v1n}) \equiv 0, \tag{19}$$

$$ml_v = l_{v1}\{f(b_{v1}) - f(b_{v2})\} + 2l_n f(b_{vv}) \equiv 0, \tag{20}$$

$$ml_n = f(b_{vv}) - f(b_{vvn}) - f(b_{v1n}) + f(b_{v2n}) \equiv 0, \tag{21}$$

$$ml_w = l_{u2} f(b_{w1}) - l_{u1} f(b_{w2}) + 2l_n f(b_{v2n}) \equiv 0. \tag{22}$$

(3) C20-Type Core

From the relations between the leg fluxes and the path fluxes,

$$b_{u2} = \phi_u - b_{u1}, \tag{23}$$

$$b_{v2} = \phi_v - b_{v1}, \tag{24}$$

$$b_{w2} = \phi_w - b_{w1}. \tag{25}$$

For nodes,

$$b_{u1n} = b_{u1} - \gamma_s\ b_{uu}, \tag{26}$$

$$b_{uv} = b_{u2} + \gamma_s\ (b_{uu} - b_{u2n}), \tag{27}$$

$$b_{uvn} = b_{u1n} + \gamma_s\ b_{u2n}, \tag{28}$$

$$b_{vv} = b_{v1} + b_{uv} - \gamma_s\ b_{v1n}, \tag{29}$$

$$b_{vvn}=b_{uvn}+\gamma_s\, b_{v1n}, \tag{30}$$

$$b_{wv}=-b_{v2}-b_{vv}+\gamma_s\, b_{v2n}, \tag{31}$$

$$b_{wvn}=-b_{vvn}-\gamma_s\, b_{v2n}, \tag{32}$$

$$b_{ww}=b_{w1n}+(b_{wv}-b_{w1})/\gamma_s, \tag{33}$$

$$b_{w2n}=b_{wvn}-\gamma_s\, b_{w1n}. \tag{34}$$

For loops,

$$ml_u=l_{v1}\{f(b_{u1})-f(b_{u2})\}+2l_n f(b_{uu})\equiv 0, \tag{35}$$

$$ml_{un}=f(b_{uu})-2f(b_{u1n})+f(b_{u2n})\equiv 0, \tag{36}$$

$$ml_{uv}=l_{uv}\{f(b_{uvn})-f(b_{uv})\}+l_n\{f(b_{u2n})-f(b_{v1n})\}\equiv 0, \tag{37}$$

$$ml_v=l_{v1}\{f(b_{v1})-f(b_{v2})\}+2l_n f(b_{vv})\equiv 0, \tag{38}$$

$$ml_{vn}=f(b_{vv})-f(b_{vvn})-f(b_{v1n})+f(b_{v2n})\equiv 0, \tag{39}$$

$$ml_{wv}=l_{uv}\{f(b_{wv})-f(b_{wvn})\}+l_n\{f(b_{v2n})-f(b_{w1n})\}\equiv 0, \tag{40}$$

$$ml_w=l_{v1}\{f(b_{w1})-f(b_{w2})\}-2l_n f(b_{ww})\equiv 0, \tag{41}$$

$$ml_{wn}=-f(b_{ww})+2f(b_{w2n})-f(b_{w1n})\equiv 0. \tag{42}$$

(4) R6-Type Core

From the relations between the leg fluxes and the path fluxes,

$$b_{r2}=b_{r3}-\gamma_s\, b_{bv}+(\gamma_s+2)\phi_v/2, \tag{43}$$

$$b_{bu}=(b_{r3}-b_{r1})/\gamma_s-b_{bv}-(\gamma_s+2)\phi_w/(2\gamma_s), \tag{44}$$

$$b_{bw}=-(b_{r3}-b_{r1})/\gamma_s+(\gamma_s+2)\phi_w/(2\gamma_s). \tag{45}$$

For loops,

$$l_{r1} f(b_{r1})-\gamma_b\{f(b_{bu})-f(b_{bw})\}\equiv 0, \tag{46}$$

$$l_{r2} f(b_{r2})+\gamma_b f(b_{bu})-f(b_{bv})\equiv 0, \tag{47}$$

$$l_{r2} f(b_{r3})+f(b_{bv})-\gamma_b f(b_{bw})\equiv 0. \tag{48}$$

When the leg fluxes ϕ_u, ϕ_v and ϕ_w are given, the wave forms of fluxes in each magnetic path of respective core can be obtained by solving the above non-linear simultaneous equations.

§ 4. Linear Solutions

When the outlines of the characteristics are cleared with the linear solutions, many useful suggestions to calculate the non-linear solution can be obtained. And it is important to clear the difference between the linear solution and the non-linear solution. Then, in this chapter, we calculate the linear solutions assuming the magnetization characteristic of Eq. (9) as the following equation, and substituting it in the fundamental equations obtained in the preceding chapter.

$$H=B/\mu, \tag{49}$$

where μ is a constant.

The calculations of this chapter are so complicated that most of them are carried out using a computer.

4.1 Calculation of the Flux Dencities

As it is linear problems, the vector symbolic method may be applied for this section. And we choose the impressed voltage $\dot{E}_u$ of the U leg as a standard of vectors.

(1) R3-Type Core

Substituting Eq. (49) into Eqs. (10) through (12), we have

$$\dot{B}_1=\{2\sqrt{3}/(\gamma_r+2)\}\dot{B}_u\ \varepsilon^{-j30^\circ}, \tag{50}$$

$$\dot{B}_2=\{2\sqrt{\gamma_r^2+\gamma_r+1}/(\gamma_r+2)\}\dot{B}_u\ \varepsilon^{-j(150+\theta)^\circ}, \tag{51}$$

$$\dot{B}_3=\{2\sqrt{\gamma_r^2+\gamma_r+1}/(\gamma_r+2)\}\dot{B}_u\ \varepsilon^{-j(270-\theta)^\circ}, \tag{52}$$

where

$$\theta=\tan^{-1}(\gamma_r-1)/\{\sqrt{3}(\gamma_r+1)\}\ (<30^\circ). \tag{53}$$

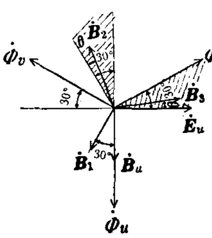

Fig. 5 Vector diagram for *R3-type* core.

Figure 5 shows the vector diagram of the fluxes ($\dot{\boldsymbol{\Phi}}_u$, $\dot{\boldsymbol{\Phi}}_v$ and $\dot{\boldsymbol{\Phi}}_w$) in each leg and the flux densities ($\dot{\boldsymbol{B}}_1$, $\dot{\boldsymbol{B}}_2$ and $\dot{\boldsymbol{B}}_3$) in each magnetic path. In Fig. 5, $\dot{\boldsymbol{B}}_u$ denotes the flux density corresponding to $\dot{\boldsymbol{\Phi}}_u$. Considering the symmetry of circuits and applied voltages, it is evident that the phase angle of $\dot{\boldsymbol{B}}_1$ is fixed constantly at $-120°$, and $\dot{\boldsymbol{B}}_2$ and $\dot{\boldsymbol{B}}_3$ are symmetric with respect to the axis, of which angle is identical with that of $\dot{\boldsymbol{B}}_1$, i. e. $-120°$. And the magnitudes of $\dot{\boldsymbol{B}}_2$ and $\dot{\boldsymbol{B}}_3$ are equal. When γ_r changes from 1 to ∞, θ varies inside the hatched extent. Figure 6 shows the relations

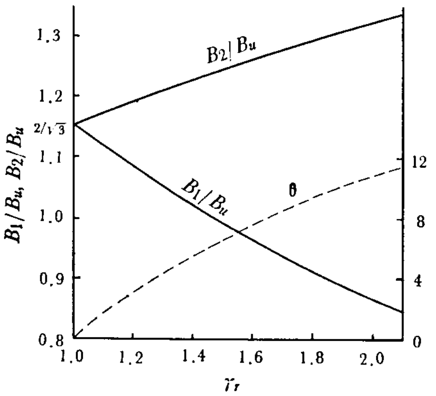

Fig. 6 Flux densities in each magnetic path and their phase angles for *R3-type* core.

between γ_r, the flux densities (B_1 and B_2) and the phase shift (θ). In the *R3-type* core, γ_b has no influence on the distribution of fluxes in the magnetic paths. When $\gamma_r = 1$, the flux densities in all paths have equal magnitudes, and they are $2/\sqrt{3}$ times greater than that in the leg, and the phase difference between them is 120° respectively. With increasing γ_r, the flux densities of inner paths increase whereas the flux density of outer path decreases. But the changing rate in $\dot{\boldsymbol{B}}_1$ is remarkable than that in $\dot{\boldsymbol{B}}_2$. On the other hand, the phase difference between $\dot{\boldsymbol{B}}_2$ and $\dot{\boldsymbol{B}}_3$ decreases gradually.

(2) C10-Type Core

From Eqs. (49), (13) through (22),

$$\dot{\boldsymbol{B}}_{u1} = \{2\sqrt{a_1^2 + a_2^2 + a_1 a_2}\, B_u/(l_{lu}\Delta)\}\, \varepsilon^{j[\tan^{-1}\{(2a_1+a_2)/\sqrt{3}a_2\} - 180]°}, \quad (54)$$

$$\dot{\boldsymbol{B}}_{u2} = \{\sqrt{(2a_1 + a_2 - 2l_{lu}\Delta)^2 + 3a_2^2}\, B_u/(l_{lu}\Delta)\} \times \varepsilon^{j\tan^{-1}\{(2a_1+a_2-2l_{lu}\Delta)/(\sqrt{3}a_2)\}}, \quad (55)$$

$$\dot{\boldsymbol{B}}_{v1} = \sqrt{\phi_{lv}^2 - 2\sqrt{3}\,\phi_{lv}\, B_u + 4B_u^2} \times \varepsilon^{j\{\tan^{-1}(\sqrt{3} - 4B_u/\phi_{lv}) + 180\}°}, \quad (56)$$

$$\dot{\boldsymbol{B}}_{v1n} = \{\sqrt{R_{n1}^2 + X_{n1}^2}/\gamma_s\}\, \varepsilon^{j\{\tan^{-1}(X_{n1}/R_{n1}) + 180\}°}, \quad (57)$$

$$\dot{\boldsymbol{B}}_{vvn} = \{4\sqrt{3}\,l_n\,(l_{lu}\,l_{v1}\,\gamma_s + l_{lv}\,l_{u2})\, B_u/(\Delta\,\gamma_s)\}\,\varepsilon^{-j120°}, \quad (58)$$

$$\dot{\boldsymbol{B}}_{vv} = (\phi_{lv} - B_{vvn})\,\varepsilon^{-j120°}, \quad (59)$$

where

$$\begin{aligned}
\phi_{lv} &= 2\sqrt{3}\,[l_{v1}\{l_{lu}\,l_{ln} - 8(l_n/\gamma_s)^2\} + 4l_{u2}\,l_n^2/\gamma_s]B_u/\Delta,\\
a_1 &= l_{u2}\{l_{lu}(l_{lv}\,l_{ln} - 4l_n^2) - 4l_{lv}(l_n/\gamma_s)^2\} + 4l_{lu}\,l_{v1}\,l_n^2/\gamma_s,\\
a_2 &= 4l_n^2\,(\gamma_s\,l_{lu}\,l_{v1} + l_{lv}\,l_{u2})/\gamma_s^2,\\
\Delta &= l_{lu}(l_{lv}\,l_{ln} - 4l_n^2) - 8l_{lv}\,l_n^2/\gamma_s^2,\\
l_{lu} &= l_{u1} + l_{u2} + 2l_n/\gamma_s,\\
l_{lv} &= 2(l_{v1} + l_n),\\
l_{ln} &= 4l_n(1+\gamma_s)/\gamma_s,\\
R_{n1} &= B_{vvn}/2 - \sqrt{3}\,a_2\,B_u/(l_{lu}\,\Delta),\\
X_{n1} &= \sqrt{3}\,B_{vvn}/2 - (2a_1 + a_2)/(l_{lu}\Delta).
\end{aligned}$$

Since the equations are too complicated, it is difficult to understand the general characters of these equations by inspection. So the vector diagram shown in Fig. 7 is drawn from the

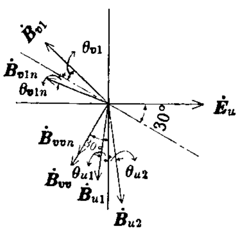

Fig. 7 Vector diagram for *C10-type* core.

results solved numerically by a computer. It is clear from the symmetry of circuits that $\dot{\boldsymbol{B}}_{w2}$, $\dot{\boldsymbol{B}}_{w1}$, $\dot{\boldsymbol{B}}_{v2}$ and $\dot{\boldsymbol{B}}_{v2n}$ correspond to $\dot{\boldsymbol{B}}_{u1}$, $\dot{\boldsymbol{B}}_{u2}$, $\dot{\boldsymbol{B}}_{v1}$ and $\dot{\boldsymbol{B}}_{v1n}$ with respect to the axis of which

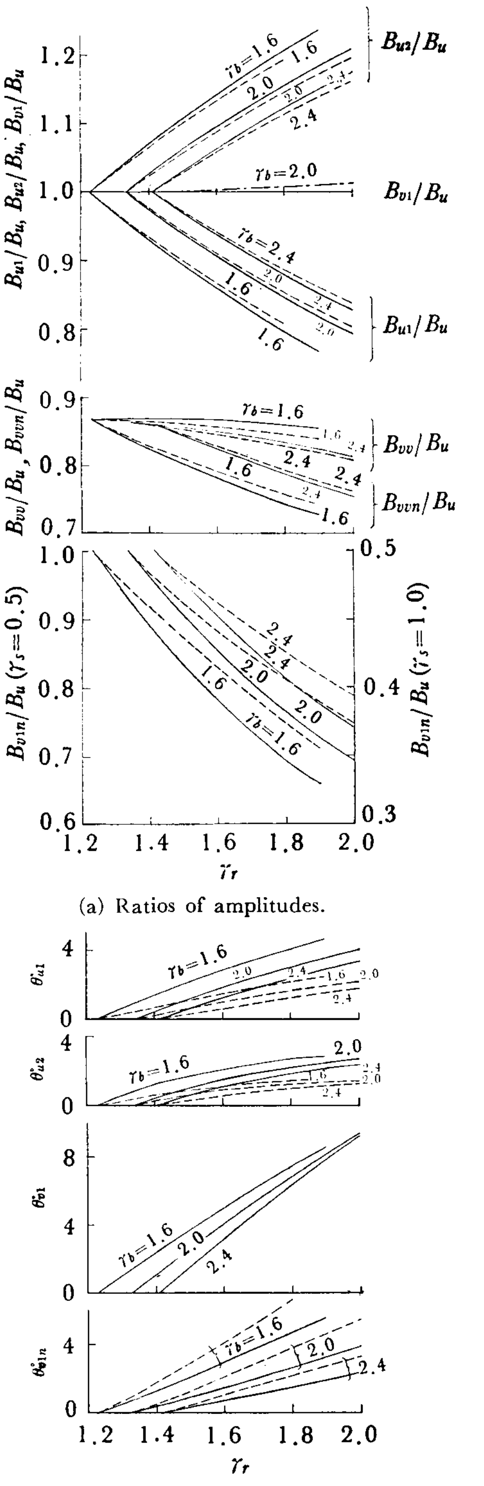

(a) Ratios of amplitudes.

(b) Variations of phase angles.

—— ; γ_s=0.5
----- ; γ_s=1.0

Fig. 8 Flux densities in each magnetic path and their phase angles for *C10-type* core.

angle is 150° (that is the phase angle of $\dot{\Phi}_v$). Therefore, $\dot{B}_{w2}$, $\dot{B}_{w1}$, $\dot{B}_{v2}$ and $\dot{B}_{v2n}$ are omitted. The phase angles of $\dot{B}_{vv}$ and $\dot{B}_{vvn}$ are fixed constantly at $-120°$.

Figure 8 shows the relations between parameters (γ_b and γ_r) and the magnitudes and phase shifts of the flux densities.

First, we consider the influences of the filling rate γ_s. With increasing γ_s, B_{u1} and B_{u2} approach the flux density B_u in the leg, but B_{v1} is hardly affected by γ_s. With increased γ_s, B_{vv} decreases and B_{vvn} increases, and consequently the difference between them will be reduced. Even if γ_s increases up to double, B_{v1n} does not reduce down to half. Increasing γ_s, θ_{u1} and θ_{u2} decrease, and the phase angles of $\dot{B}_{u1}$ and $\dot{B}_{u2}$ approach that of the flux density $\dot{B}_u$ in the U leg, that is $-90°$. θ_{v1} is hardly affected by γ_s. With increasing γ_s, θ_{v1n} also increases.

Then, we consider the influences of the parameters γ_b and γ_r. When γ_r decreases and γ_b increases, B_{u1} and B_{u2} approach B_u, and B_{v1u} increases up to B_u at $\gamma_s=0.5$ and up to half of B_u at $\gamma_s=1.0$. B_{v1} is hardly affected by γ_b and γ_r. Increasing γ_b and decreasing γ_r, B_{vv} and B_{vvn} approach $\sqrt{3}\,B_u/2$. When γ_b increases and γ_r decreases, θ_{u1}, θ_{u2}, θ_{v1} and θ_{v1n} decrease, and the phase angles of $\dot{B}_{u1}$ and $\dot{B}_{u2}$ approach that of $\dot{B}_u$, i.e. $-90°$. And the phase angles of $\dot{B}_{v1}$ and $\dot{B}_{v1n}$ approach that of the flux density $\dot{B}_v$ in the V leg, i.e. 150°.

A summary of the facts described above is shown below.

Increasing γ_b and decreasing γ_r, the flux distribution approaches that in the *B-type* core. Increasing γ_s, the flux distribution is a little improved when γ_b is small and γ_r is large. $\dot{B}_{v1n}$ which is directly affected by γ_s changes very much, whereas the magnetic characteristics of this core are hardly improved by increasing γ_s, because the volume through which B_{v1n} passes is very small comparing with total volume of core. If one wishes the value of B_{v1n} becomes comparable to the flux density in the leg, γ_s should be about 0.5. However, the most suitable filling rate γ_s should be decided to minimize the core loss. This problem will be discussed later. The filling rate of the part through which B_{vv} passes should be about 100%, because B_{vv} is approximately equal to the flux density in the leg when $\gamma_s=1.0$.

On actual transformer core, increasing the flux density, the differences in magnetic reluctances of each branch become smaller with saturation of magnetic path. Hence, it may be assumed that γ_b and γ_r are equal to 1. Using this assumption, the following solutions are obtained.

$$\left.\begin{aligned} &B_{u1}=B_{u2}=B_{v1}=B_u,\\ &\theta_{u1}=\theta_{u2}=\theta_{v1}=\theta_{v1n}=0,\\ &B_{vv}=B_{vvn}=\sqrt{3}\ B_u/2,\\ &B_{v1n}=B_u\cdots\cdots(\text{at } \gamma_s=0.5),\\ &\quad\ =B_u/2\cdots(\text{at } \gamma_s=1.0). \end{aligned}\right\} \qquad (60)$$

(3) C20-Type Core

To find the solutions, we must solve the simultaneous equations consisting of the twenty-one dimensions of the first order, i.e. Eq. (49) and Eqs. (23) through (42). These calculations are so tedious that the numerical analysis by a computer is applied. That is; increasing the phase angle ωt by step 0.2°, these simultaneous equations are solved numerically, and the wave forms of the fluxes in each magnetic path are obtained. Applying the Fourier's analysis to these wave forms, the magnitudes and phase angles of the fluxes are calculated.

The vector diagram obtained from these results is shown in Fig. 9. In this case, like the *C10-type*, the vectors $\dot{B}_{w2}$, $\dot{B}_{w1}$, $\dot{B}_{ww}$, $\dot{B}_{w2n}$, $\dot{B}_{w1n}$, $\dot{B}_{wv}$, $\dot{B}_{wvn}$, $\dot{B}_{v2}$ and $\dot{B}_{v2n}$ correspond to $\dot{B}_{u1}$, $\dot{B}_{u2}$, $\dot{B}_{uu}$, $\dot{B}_{u1n}$, $\dot{B}_{u2n}$, $\dot{B}_{uv}$, $\dot{B}_{uvn}$, $\dot{B}_{v1}$ and $\dot{B}_{v1n}$ with respect to the axis, of which angle is 150°. Of course, the phase angles of the vectors $\dot{B}_{vv}$ and $\dot{B}_{vvn}$ are constant at $-120°$.

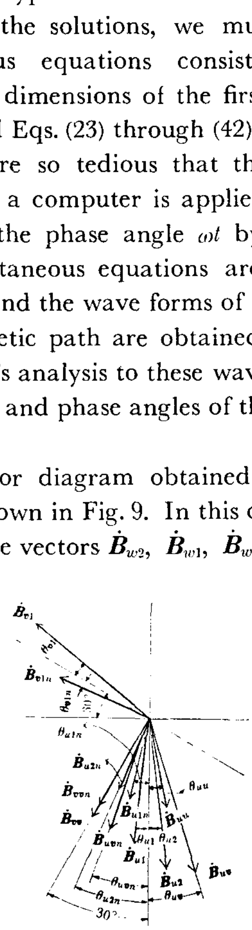

Fig. 9 Vector diagram for *C20-type* core.

Figure 10 shows the relations between parameters (γ_b and γ_r) and the magnitudes and phase shifts of the flux densities. The tendency how B_{u1}, B_{u2}, B_{v1}, B_{vv}, B_{vvn}, and B_{v1n} are changed according to γ_s, γ_b and γ_r almost coincides with that of the *C10-type* core. But the distribution of B_{u1} and B_{u2} is more uniformly improved than that in the *C10-type* core. The variation of B_{v1n} with γ_s, γ_b and γ_r is greater than that in the *C10-type* core. Though the tendency of variations of B_{uvn} and B_{uv} is similar to B_{u1} and B_{u2}, the flux distribution of the group of B_{uvn} and B_{uv} is less balanced than that of B_{u1} and B_{u2}. Even if γ_s decreases down to half, B_{u2n} and B_{uu} do not increase up to double, and they remain fairly small. Hence, for the similar reason to the case found in the *C10-type* core, the value of γ_s is sufficient at 0.5. Figure 10 shows the filling rate of the part, through which B_{uu} passes, should be about 100%. The values of B_{u1n} and B_{uu} are considerably affected by γ_s.

Consequently, the flux distribution in this type core is more improved than that in the *C10-type* core, and is similar to that in the *B-type* Core. *

For the phase angles, θ_{u1} and θ_{u2} have the same tendency as those of the *C10-type* core. Their values are below 1° when $\gamma_s=0.5$ and are nearly zero when $\gamma_s=1.0$. θ_{v1} almost agrees the value of the *C10-type*, and θ_{v1n} takes a negative value when γ_b and γ_r become larger.

If γ_b and γ_r are equal to 1,

$$\left.\begin{aligned} &B_{u1}=B_{u2}=B_{v1}=B_{uv}=B_{uvn}=B_u,\\ &B_{vv}=B_{vvn}=\sqrt{3}B_u/2,\\ &\theta_{u1}=\theta_{u2}=\theta_{v1}=\theta_{v1n}=\theta_{uv}=\theta_{uvn}\\ &\quad=\theta_{u1n}=\theta_{u2n}=\theta_{uu}=0. \end{aligned}\right\}$$

* The flux distribution in the *B-type* core is practically not uniform. The flux density at the part near the window is higher than that far from the window. We still assume it is the uniform distribution.

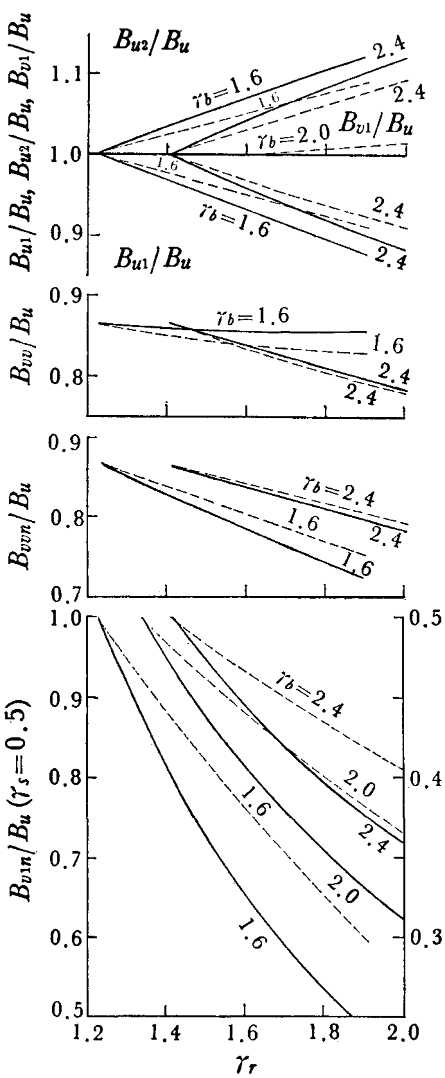

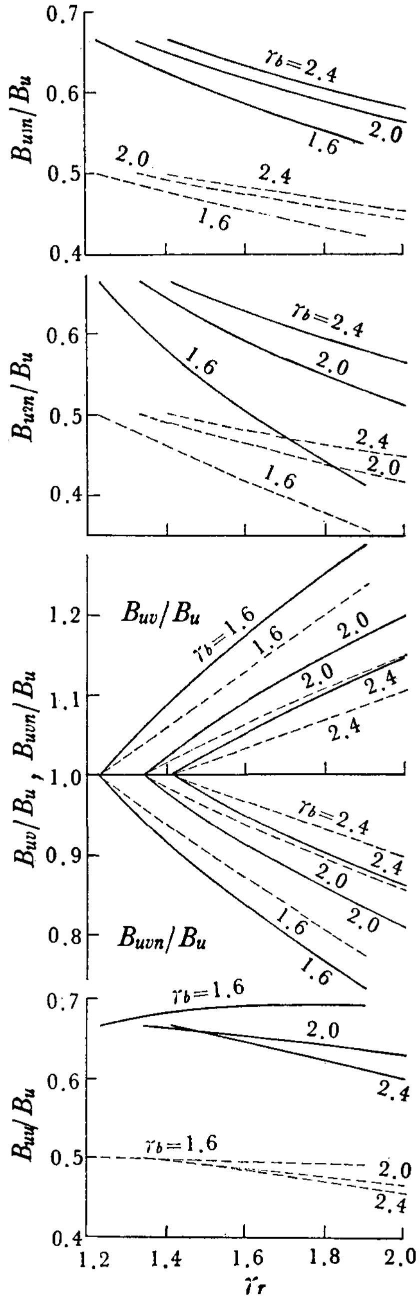

(a) Ratios of amplitudes.

$$
\left.
\begin{aligned}
&\text{And if } \gamma_s = 0.5, \\
&\quad B_{v1n} = B_u, \\
&\quad B_{u1n} = B_{u2n} = B_{uu} = 0.667\ B_u. \\
&\text{If } \gamma_s = 1.0, \\
&\quad B_{v1n} = B_u/2, \\
&\quad B_{u1n} = B_{u2n} = B_{uu} = B_u/2.
\end{aligned}
\right\} \quad (61)
$$

The two fluxes* such as $\dot{B}_1$ and $-\dot{B}_2$, $\dot{B}_2$ and $-\dot{B}_3$, $\dot{B}_{u1}$ and $\dot{B}_{u2}$, $\dot{B}_{v1}$ and $\dot{B}_{v2}$ and $\dot{B}_{uv}$ and $\dot{B}_{uvn}$, of which vector-sum forms the flux in the leg, have the following relations between the magnitude and phase angle. These relations

* As the sectional area of the path is unity here, the flux density is equivalent to the flux.

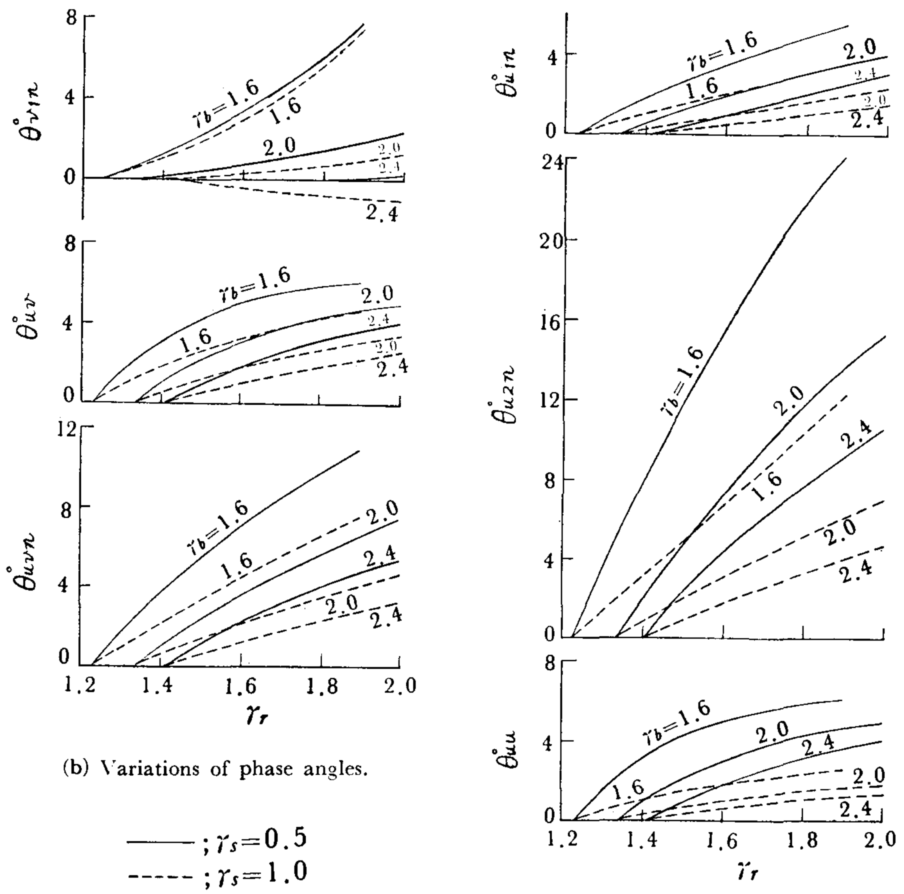

Fig. 10 Flux densities in each magnetic path and their phase angles for *C20-type* core.

are still valid as to the fundamental harmonics in the case of non-linear.

Now, let us represent the pair of fluxes mentioned above by $\dot{B}_a(=B_a\,\varepsilon^{j\theta_a})$ and $\dot{B}_b\,(=B_b\,\varepsilon^{-j\theta_b})$ and the leg flux by $2\dot{B}_u$. The following equation is obtained.

$$2\dot{B}_u=B_a\,\varepsilon^{j\theta_a}+B_b\,\varepsilon^{-j\theta_b}. \tag{62}$$

The relationship among those vectors is shown in Fig. 11, where the base of the vectors is $\dot{B}_u$. From Fig. 11, the following equations are obtained.

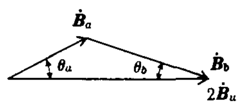

Fig. 11 Relation between flux in the leg and those of individual magnetic paths.

$$\cot\,\theta_b=\frac{2}{(B_a/B_u)\sin\,\theta_a}-\cot\,\theta_a, \tag{63}$$

$$\frac{B_b/B_u}{B_a/B_u}=\sin\,\theta_a/\sin\,\theta_b. \tag{64}$$

The magnitudes and phase angles in Figs. 6, 8 and 10 satisfy the relationships of Eqs. (63) and (64). On the V leg, additional equations are satisfied from symmetry of the circuit.

$$B_{v1}=B_{v2},\quad \theta_{v1}=\theta_{v2}.$$

Hence, from Eqs. (63) and (64),

$$\cos\theta_{v1}=\frac{1}{B_{v1}/B_u}. \tag{65}$$

(4) R6-Type Core

From Eqs. (43) through (49),

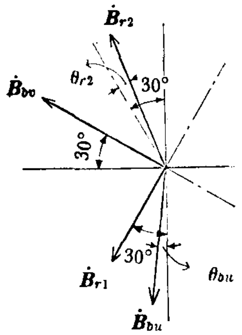

Fig. 12 Vector diagram for *R6-type* core.

$$\dot{B}_{r1}=\sqrt{3}\,\gamma_b(\gamma_s+2)l_{r2}B_u\varepsilon^{-j120^\circ}/\{\gamma_b(l_{r1}+2l_{r2})+\gamma_s l_{r1} l_{r2}\}, \tag{66}$$

$$\dot{B}_{r2}=[-\sqrt{3}\{(\gamma_b+2)\gamma_b+\gamma_s l_{r1}\}l_{r2}+j\{(\gamma_b+2)(2l_{r1}+l_{r2})\gamma_b+\gamma_s(2\gamma_b+1)l_{r1} l_{r2}\}]B_u/\Delta_6, \tag{67}$$

$$\dot{B}_{bu}=[\sqrt{3}(\gamma_b l_{r2}-l_{r1})-j\{(2l_{r1}+l_{r2})\gamma_b+3l_{r1}+2\gamma_s l_{r1} l_{r2}\}]l_{r2}B_u/\Delta_6, \tag{68}$$

$$\dot{B}_{bv}=(\gamma_s+2)l_{r2}B_u\varepsilon^{-210^\circ}/(\gamma_b+\gamma_s l_{r2}+2), \tag{69}$$

where

$$\Delta_6=2\{\gamma_b(l_{r1}+2l_{r2})+\gamma_s l_{r1} l_{r2}\}\{\gamma_b+\gamma_s l_{r2}+2\}/(\gamma_s+2).$$

In the vector diagram shown in Fig. 12, the phase angles of $\dot{B}_{r1}$ and $\dot{B}_{bv}$ are constant at $-120°$ and $150°$ respectively. The vectors $\dot{B}_{r2}$ and $\dot{B}_{r3}$ are symmetric with respect to the axis, of which angle is identical with the phase angle of $\dot{B}_{r1}$. The vector $\dot{B}_{bu}$ corresponds to $\dot{B}_{bw}$ with respect to the axis, of which angle is identical with the phase angle of $\dot{B}_{bv}$ i. e. 150°.

Figure 13 shows the relations between param-

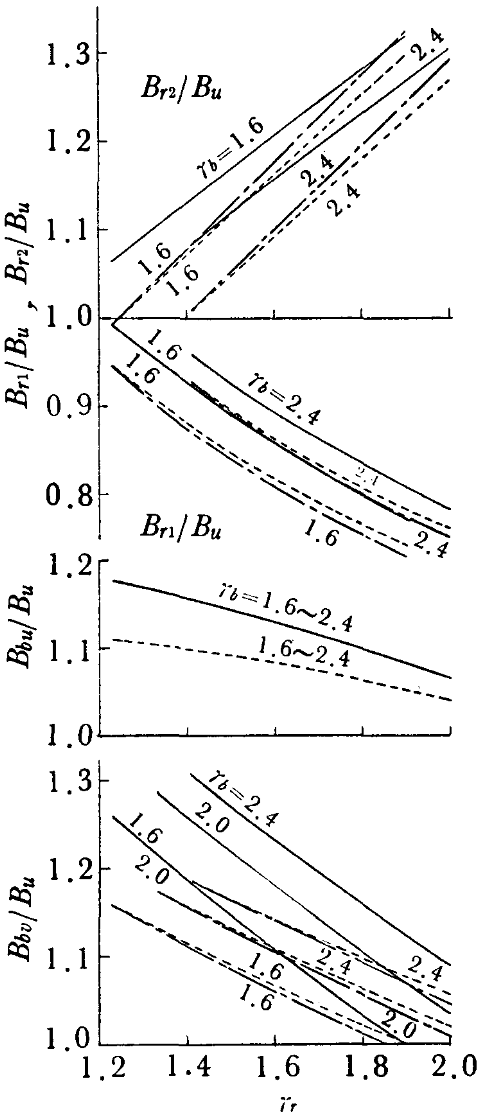

(a) Ratios of amplitudes.

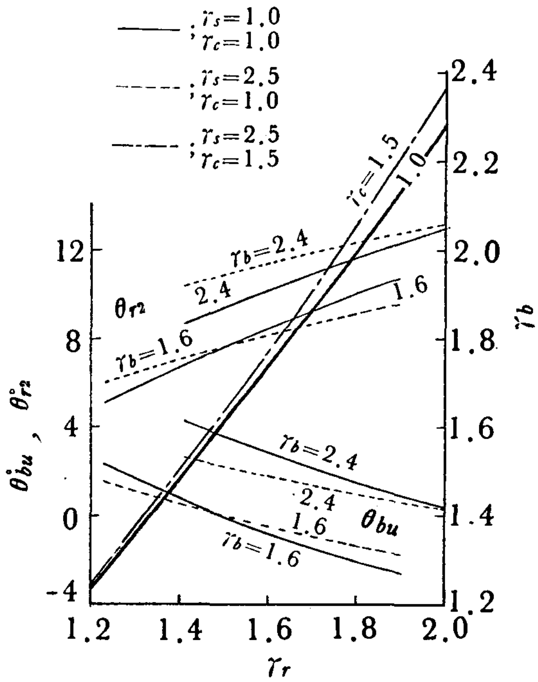

(b) Variations of phase angles, and relations between γ_r and γ_b (thick-lines) which satisfy the equation (70).

Fig. 13 Flux densities in each magnetic path and their phase angles for *R6-type* core.

eters and the magnitudes and phase shifts of the flux densities. With decreasing parameters γ_c and γ_r, and increasing parameter γ_b, B_{r1} and B_{r2} approach the flux density B_u in the leg. They become smaller when γ_s is increased. Increasing parameters γ_c, γ_s and γ_r, and decreasing parameter γ_b, B_{bv} decreases. B_{bu} is hardly affected by γ_c and γ_b, and it decreases when γ_s and γ_r increase.

When the sectional area of the central path, through which b_{bu}, b_{bv} and b_{bw} pass, increases, the flux densities B_{r1}, B_{r2} and B_{r3} decrease, not to mention the flux densities B_{bu}, B_{bv} and B_{bw} in these parts.

For the phase angles, θ_{r2} is greater than θ of the *R3-type* core and it is hardly affected by γ_c. It decreases when γ_c, γ_b and γ_r decrease. When γ_b becomes larger and γ_r becomes smaller, θ_{bu} changes the sign from negative to positive. In Fig. 13 (b) the thick-lines show the relation between γ_r and γ_b which satisfies the condition of $\theta_{bu}=0$; that is, the condition in which $\dot{B}_{bu}$ becomes in-phase with $\dot{B}_u$. Equation (70) is obtained from this condition.

$$\gamma_r=\gamma_b\{\gamma_c(5\gamma_b+3)+6\gamma_b+2\}/\{\gamma_c(\gamma_b^2+5\gamma_b+2)+6\gamma_b+2\}. \tag{70}$$

The usual extent of γ_s, γ_c etc. is mentioned in detail in the chapter 5.

4.2 Calculation of Core Losses

As the wave forms of the fluxes in each magnetic path have been known by solving the fundamental equations, the maximum value (B_m), the effective value (B_e), the magnitudes (B_{ki}) of minor loops etc. are obtained. Hence, the core loss $\boldsymbol{W}$ (W/kg) can be calculated using the following equations[6].

$$\boldsymbol{W}=\boldsymbol{W}_h+\boldsymbol{W}_e, \tag{71}$$

$$\boldsymbol{W}_h=w_h(B_m)+2\sum w_h(B_{ki})^*, \tag{72}$$

$$\boldsymbol{W}=w_e(B_e), \tag{73}$$

where

$\boldsymbol{W}_h$: hysteresis loss (W/kg)
$\boldsymbol{W}_e$: eddy current loss (W/kg)
$w_h(B_m)$: hysteresis loss caused by the maximum flux density B_m (W/kg)
$w_e(B_e)$: eddy current loss caused by the flux density B_e (W/kg)

B_e is the maximum flux density of the sinusoidal wave which has the same effective voltage as that corresponding to the distorted flux. Hence, B_e is defined by the following equation.

$$B_e=\sqrt{\sum(n\,B_n)^2}, \tag{74}$$

where B_n is the magnitude of the n-th harmonic component.

In this paper, only the linear solution is handled. Therefore, $B_m=B_e$ and $B_{ki}=0$, and it is not necessary to divide the core loss into hysteresis and eddy current losses.

Let us consider the core-loss ratio σ defined by the following equation.

$$\sigma=\boldsymbol{W}/w(B_u), \tag{75}$$

where $\boldsymbol{W}$ is the core loss of the objective core which is now being studied, and $w(B_u)$ is the core loss of the *B-type* core. The flux density B_u in the leg of the *B-type* core is the same as

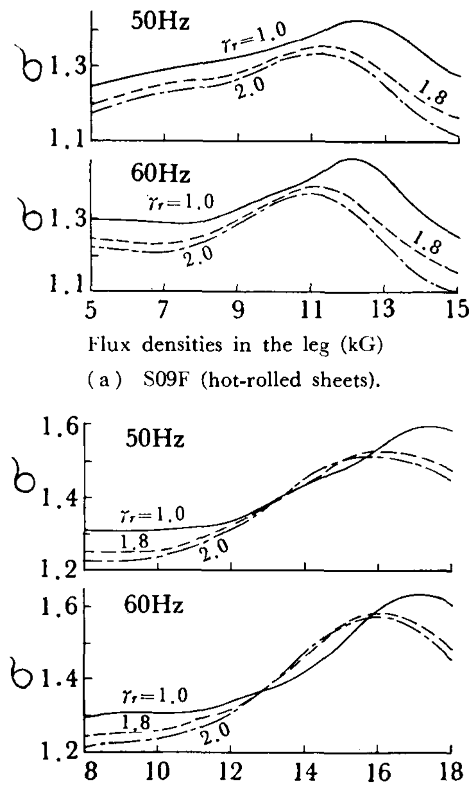

(a) S09F (hot-rolled sheets).

(b) G10 (cold-rolled strip steel).

Fig. 14 Core-loss ratios for *R3-type* core.

* Figure $\sum$ represents the summation of losses caused by the minor loops which appear in a half cycle successively.

that in the leg of the objective core. So, σ denotes the core-loss ratio where the core loss of the *B-type* core is taken as a standard comparing with that of other type of cores. The core-loss ratios σ for various type core are shown as follows.

(1) R3-Type Core[8]

$$\sigma=\{\gamma_r w(B_1)+2w(B_2)\}/\{(\gamma_r+2)w(B_u)\}. \tag{76}$$

As shown in Fig. 14, the core-loss ratio (Fig. 14 (b)) for the core made of cold-rolled strip steel is greater than that (Fig. 14 (a)) made of hot-rolled sheets. At usual operating flux densities of the core with usual dimensions, the value of σ is roughly 1.1~1.2 for S09F*, and 1.50~1.58 for G10. **

The core-loss ratio changes broadly according to the shape of core-loss curve ($w(B)$).

(2) C10-Type Core

$$\sigma=[2\{l_{u1}w(B_{u1})+l'_{u2}w(B_{u2})+l'_{v1}w(B_{v1})+l_n w(B_{r1n})\}+l_n\{w(B_{vr})+w(B_{rvn})\}]/\{2(l_{u1}+l'_{u2}+l'_{r1}+2l_n)w(B_u)\}, \tag{77}$$

where

$$l'_{u2}=l_{u2}-l_n/2,$$
$$l'_{r1}=1-3l_n/2.$$

To avoid overlap of the areas at upper and lower parts of the V leg, the magnetic path lengths l'_{u2} and l'_{r1} are used instead of l_{u2} and l_{v1}.

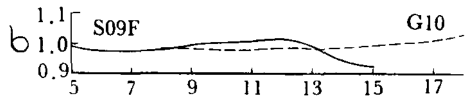

Fig. 15 Core-loss ratios for *C10-type* core.

Figure 15 shows an example of core-loss ratios. The core-loss ratio is hardly affected by parameters such as γ_b, γ_r, γ_s and frequency, especially by γ_s. As γ_s has no influence on the core-loss ratio, the filling rate of this type core is sufficient at 0.5. The core loss of this type is fairly the same value as that of the *B-type* core.

* Hot-rolled sheets : JIS C 2551—70 (grade : AISI-68 M-14)

** Cold-rolled strip steel : JIS C 2553—70 (grade : AISI-68 M-5)

The reason why core-loss ratio is sometimes smaller than 1 depends on the fact that the flux distribution of the *B-type* core is assumed uniform.

(3) C20-Type Core

As mentioned in the preceding section, the flux distribution in this type core is more improved than that in the *C10-type*. Therefore, this type core gives almost the same core loss as the *B-type*.

(4) R6-Type Core[7]

$$\sigma=[l_{r1}w(B_{r1})+2l_{r2}w(B_{r2})+\{2l'_{bu}w(B_{bu})+l'_{bv}w(B_{bv})\}\gamma_s]/[\{l_{r1}+2l_{r2}+(2l'_{bu}+l'_{bv})\gamma_s\}w(B_u)], \tag{78}$$

where

$$l'_{bu}=l_{bu}-\{2+\gamma_{rb}(\gamma_r-2)\}\gamma_c/\{24(\gamma_c+2)\},$$
$$l'_{bv}=1-\{2+\gamma_{rb}(\gamma_r-2)\}\gamma_c/\{12(\gamma_c+2)\}.$$

The reason why the path lengths l'_{bu} and l'_{bv} are used instead of l_{bu} and l_{bv} is the same as the case of the *C10-type* core.

The core-loss ratios at 60Hz and at $\gamma_c=1$ are shown in Fig. 16. The ratio is hardly affected by γ_c. The difference of ratios between 50Hz and 60Hz is very small. The reason why the larger γ_s becomes, the smaller σ becomes is explained from the increase of volume corresponding to the *B-type* core.

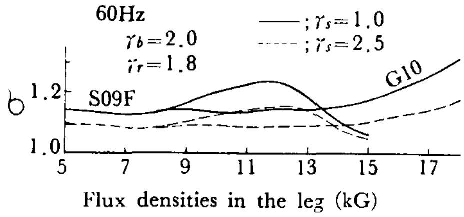

Fig. 16 Core-loss ratios for *R6-type* core.

When the core quality is S09F, σ is between 1.06 and 1.24 at $\gamma_s=1.0$ and is between 1.04 and 1.15 at $\gamma_s=2.5$. When the core quality is G10, σ is between 1.13 and 1.37 at $\gamma_s=1.0$ and is between 1.09 and 1.24 at $\gamma_s=2.5$. To find Figs. 14, 15 and 16, the loss curve which is obtained from the Epstein tester using parallel specimen is used as the function $w(B)$ in Eq. (75). Generally, the core loss of the *B-type* core is a little greater than that of Epstein tester. Therefore, strictly speaking, σ in Figs. 14, 15 and 16 is the core-loss ratio of which base is the core loss measured by the

Epstein tester.

§ 5. Parameters γ_s and γ_c in R6-Type Core

The *R3-type* core is recognized as a special type in the *R6-type* core of which parameters γ_s and γ_c converge to zero. Therefore, Eqs. (50) and (51) can be also obtained by substituting these conditions into Eqs. (66) and (67). Similarly, the *B-type* core is regarded as a special type in the *R6-type* core of which parameters γ_s and γ_c are going to be of the limitted infinity.

When we reexamine the *R6-type* core from this point of view, the following facts may be understandable. That is ; in Fig. 13 if γ_s and γ_c approach zero, $\dot{B}_{r1}$ and $\dot{B}_{r2}$ come close to $\dot{B}_1$ and $\dot{B}_2$ of the *R3-type* core shown in Fig. 6. One should notice here that this tendency will not always occur if only γ_c becomes small. γ_s and γ_c become necessarily small at the same time. As the cross section of the power transformer-core commonly used is approximately circular as shown in Fig.17, γ_s and γ_c are related

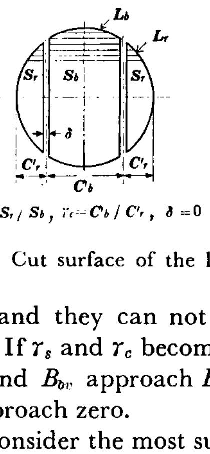

Fig. 17 Cut surface of the leg.

to each other and they can not be changed independently. If γ_s and γ_c become larger, the values of B_{bu} and B_{bv} approach B_u and their phase shifts approach zero.

Next, let us consider the most suitable value of γ_s. Though the cross section of an actually used transformer core is made of a polygon which is inscribed in a circle, we consider it approximately as a circle. For the preceding definition on γ_c is inadequate, we introduce here the following parameter γ'_c instead of γ_c.

$$\gamma'_c = C'_b / C'_r, \tag{79}$$

where C'_b and C'_r are defined in Fig. 17. If the cross section is a circle, there is a relation between γ_s and γ_c as shown in Fig. 18.

From the view-point of cooling, let us reconsider the most suitable value of γ_s. In

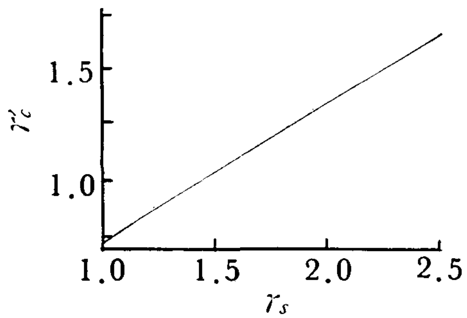

Fig. 18 Relation between γ_s and γ'_c for circular section.

silicon steel sheets, the longitudinal thermal conductivity is nearly ten times larger than the transverse thermal conductivity. To simplify, we assume here that the thermal conductivity is uniform in all directions, and heat is generated uniformly in the core by virtue of the core loss. Then, the following equation must be made in order to satisfy that rise of temperature in respective paths is uniform.

$$L_b / L_r = \gamma_s, \tag{80}$$

where L_b and L_r are the circumferences of the cross sections in respective magnetic paths (see Fig. 17). Equation (80) is satisfied when $\gamma_s = 1.11$ and $\gamma'_c = 0.8$.

While, as it was stated previously, it is desirable to make the value of γ_s as large as possible if one wishes to decrease the core loss.

In most transformer actually used, from various circumstances, the value of γ_s is in between 2.2 and 2.4 and that of γ'_c between 1.4 and 1.6.

§ 6. Conclusions

With regard to the flux distribution in a transformer core, only linear solutions have been given for restricted constructions, because of the complication to analyse the magnetic circuits. Then, authors have analysed many complicated cores using a computer, and obtained the following results.

(1) The fundamental equations for magnetic circuits are established.
(2) The vector diagrams for each type core are obtaind.
(3) The relations between the parameters concerning core shape and amplitudes and phase angles of the fluxes in each magnetic path are cleared.

(4) The magnetic characteristics of the *R3-type* core are not affected by the parameter γ_b.

(5) Except for the *R3-type* core, the core-loss ratio is hardly affected by the parameters γ_b and γ_r. The influence of core quality (i. e. core-loss curve) on the core-loss ratio is remarkable, but the influence of frequency on it is less remarkable.

(6) Even the *C10-type* core of which parameter γ_s is equal to 0.5 has almost the same magnetic characteristics as the *B-type* core. Hence, it is not necessary to make a core magnetically coupled more closely (i. e. $\gamma_s > 0.5$), because such core needs much labors to construct.

(7) The *C20-type* core is unsuitable comparing to the *C10-type* from the standpoints of cooling and cost.

(8) The *R6-type* core has an advantage having characteristics (such as core loss, exciting current) situated in between the *R3-type* core and the *B-type*. The more the sectional area of central path increases, the more the core loss decreases. The core loss is hardly affected by the parameter γ_c.

The above conclusions have been drawn on an assumption that the magnetization characteristic is linear. The non-linear solutions and experimental results will be reported in elsewhere[7),8)].

The authors would like to acknowledge the continuous guides and encouragements from Prof. Mine.

References

1) M. VIDMAR : *Die Transformatoren*, 360 (1956).
2) ARNOLD-la-COUR : *Die Transformatoren*, 225 (1936).
3) R. KÜCHLER : *Die Transformatoren*, 37 (1966).
4) S. YAMAGUCHI : Journal of the Institute of Electrical Engineers of Japan, **86** (1966) No. 5, 820.
5) S. YAMAGUCHI : Ibid., **87** (1967) No. 6, 1161.
6) T. NAKATA, Y. ISHIHARA and M. NAKANO: Electrical Eng. in Japan, **90** (1970) No. 1, 10.
7) T. NAKATA, Y. ISHIHARA and M. NAKANO : Journal of the Institute of electrical Engineers of Japan, **91** (1971) No. 5, 877.
8) T. NAKATA, Y. ISHIHARA and M. NAKANO : 1969 Joint Convention Record of Four Institutes of Electrical Engineers, Japan, No. 627.